MICRO-RAMAN MAPPING OF MINERAL PHASES IN THE STRONGLY SHOCKED TAIBAN ORDINARY CHONDRITE. T. E. Acosta[1], E. R. D. Scott[2], and S. K.Sharma[2], [1]Department of Geology & Geophysics, University of Hawaii, Honolulu, HI 96822, USA (tayro@hawaii.edu); [2]Hawaii Institute of Geophysics and Planetology, University of Hawaii, Honolulu, HI 96822.

Introduction: During the formation and later evolution of the Solar System, asteroids have repeatedly collided with each other and with larger bodies triggering shock waves [1]. Meteorites that have undergone such shock waves show different shock effects depending on the peak pressures and temperatures, and duration of the collision events [2]. Taiban is a very strongly shocked, shock stage S6 [1], ordinary L5 chondrite found in New Mexico in 1934. It has been classified as a black and veined [3] since it shows opaque shock melt. The meteorite is relatively unweathered, with minor amounts of iron oxide of terrestrial origin present in thin veins and around metallic Fe-Ni grains. The melt vein is opaque microscopically in transmitted light and contains small inclusions of metallic Fe-Ni-troilite assemblages, intermingled with transparent but highly shock-altered and often mosaicized relict silicates [4].

Micro-Raman spectroscopy has been used to provide univocal identification of minerals and glassy phases in meteorites as well as a tool to obtain additional information on structural and compositional variations inside mineral grains [5]. Raman mapping of the sample mounted on an automated X-Y-Z stage allows visualization of mineralogical information included in the Raman spectra [6]. We have studied the polished thin section UNM297 of Taiban meteorite with micro-Raman spectroscopy and Raman mapping to identify major and minor mineral phases in the thin-section.

Experimental set-up. All spectra were acquired with a Kaiser Optical Systems' Micro-Raman instrument using 785 nm laser excitation, 10 mW laser power and 150 s exposure time. The spatial resolution was 3 μm with 100x objective, and the stage spatial resolution was 1 μm. The mapped areas shown in Fig. 1 are aproximately 30 x 25 μm^2 and contain 144 points. The Raman spectra of the mapped area are composed mainly of first order Raman peaks allowing us to deconvolute single phase maps. Mapping the area over the baseline for characteristic spectral peaks yields separation of phases. Each phase field is then turned into a overlay of different color that can be combined into a composite image creating the Raman images. Reflection and transmission optical micro-photographs are used to put every spectral image into context.

Results: The micro-photograph of the polished thin section UNM297 of Taiban meteorite is shown in Fig. 1. The visual appearance of the transparent silicate pockets is dominated by blue ringwoodite crystals. The white matrix is composed mainly of pyroxene and plagioclase converted to its shock induced glass form, maskelynite [7].

The single-point Raman spectra (Fig. 2) and spectra for Raman imaging area were taken in and around the biggest ringwoodite crystal. Raman spectra measured in the inner part of the crystal show the Raman fingerprints of pure ringwoodite. The peaks located at 301, 596, 799, 844 cm^{-1} are Raman fingerprints of ringwoodite $(Fe,Mg)_2Si0_4$. These Raman fingerprints

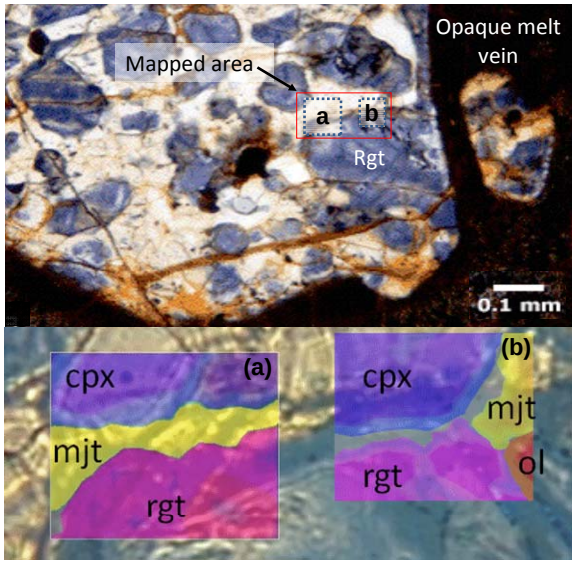

Fig 1: (Top) Transmitted light micrograph of the studied shocked lithic pocket inside the melt vein. Rectangles (a and b) mark the Raman mapping areas. (Bottom) Raman images of the two different marked areas along the phase boundary between the ringwoodite grain and the pyroxene-majorite assemblage. Different color correspond to integration over different spectral features, 697 cm^{-1} calcium pyroxene (cpx), 596 cm^{-1} majorite (mjt), 843-876 cm^{-1} ringwoodite (rgt) and 855 cm^{-1} olivine (ol) (see text for explanation).

have also been observed in natural ringwoodite lamellae in Sixiangkou meteorite [8, 9]. The intensity of the 876 cm^{-1} line is very much spatial dependent. It is smaller (around one tenth the intensity of the main 799, 844 cm^{-1} lines) in pure ringwoodite found in the interior of the crystal and it becomes the main peak as other Raman signals of the original olivine, intermediate wadsleyite phase and of other unknown phases

are also present, i.e., the peak is stronger where the

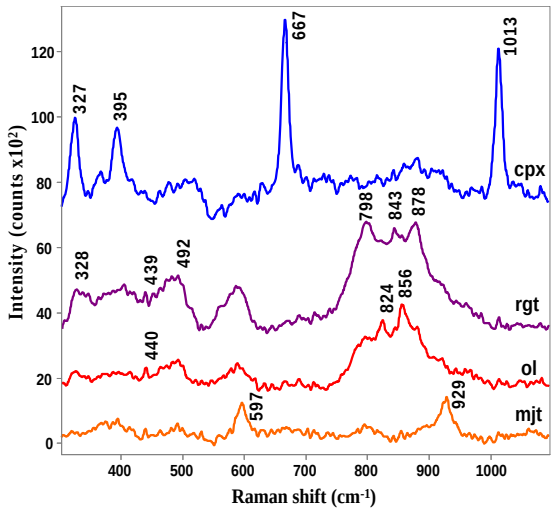

Fig. 2: Raman spectra of $(Mg, Fe)_2SiO_4$ (olivine), $(Mg, Fe)_2SiO_4$ with the spinel structure (ringwoodite), calcium pyroxene (augite) and pyroxene with the garnet structure (majorite) in the frequency region, 200 to 1200 cm^{-1}. Spectra are typical spectra for each phase extracted from the spectral image data points. Integration time of 150s. Laser 785 nm, 10 mW.

solid-state phase transition was not fully accomplished. The same peak was observed by other worker [11,12] and it could be due to a defect induced vibrational mode, to a inverse spinel structure in which the Mg and Fe ions are both in fourfold and six fold coordination, or to the presence of glassy material. At several points in and around the ringwoodite, Raman signatures of the original olivine are found. Raman spectra of the grains within the ringwoodite and between grains show the characteristics peaks of olivine at 824 and 856 cm^{-1}, close to the typical shift found in forsterite, 824, 856 cm^{-1} [13], this pair originates from the Si-O_{nb} bond stretching in the $[SiO4]^{4-}$ tetrahedral [14]. Additional olivine peaks appear at 301, 329, 340, 424, 547, 610 and 967 cm^{-1} in the olivine within the ringwoodite and in the olivine filling the 1µm crack between the ringwoodite grains. Olivines were found in contact with the ringwoodite crystal; pyroxene assemblages or the melt vein are in direct contact with the ringwoodite around the rest of the perimeter. The composition of the olivine is 88% forsterite within the ringwoodite and 94% in the crack, according to a Raman compositional calibration of olivines [14].

White grains show pyroxene Raman fingerprints, precisely of the mineral augite/diopside (*C*2/*c* monoclinic pyroxene): two intense peaks, the first one at 1013 cm^{-1} corresponding to the Si-O_{nb} bond stretching in the $[SiO4]^{4-}$ unit, and the second one at 667cm^{-1} corresponding to the bridging oxygen stretch in the Si-O_b-Si bond of the $[Si_2O_6]^{4-}$ unit. Three smaller peaks are present in the range 300-400 cm^{-1}, 327, 369 and 395 cm^{-1} created by the displacements of cations from their equilibrium lattice positions [5]. Along with the pyroxene crystals, majorite assemblages are present in the white matrix. Modes of majorite are found at 396, 599, 800, 929, and 1064 cm^{-1} [15] Majorite is the cubic garnet polymorph of pyroxene. It has previously found in Coorara, Catherwood, Pampa del Infierno, Tenham, Sixiangkou and Peace River chondritic meteorites. Majorite forms in these meteorites from low-Ca, high-Al pyroxenes, olivines and shock induced glass. The peak positions of the majorite are in great accordance with the [15] for pure $MgSiO_3$; however there is a significant line width increase in several of the measured crystals, possibly due to some deformational stress in the crystals. The pyroxene-majorite assemblages completely surround the ringwoodite crystals in the silicate pocket suggesting that under the pressure and temperature conditions that the silicate pocket experienced, all the enstatite transformed into the its high pressure phase majorite, whereas the calcium pyroxene reversed a high pressure transformation after the shock or it remained unchanged.

Summary: Raman mapping allowed identification of minor phases in the thin section of Taiban meteorite, and also revealed for the first time strained phases of ringwoodite at the mineral boundaries.

Acknowledgment: This work was supported in part by NASA under a MIDDP grant NNX07AV44G.

References: [1] Raymond, S. N. (2010) Formation of Terrestrial Planets. Ch 6 in R. Barnes, Wiley-VCH. [2] Stöffler D. et al. (1991) *Geochim. Cosmochim. Ac. 55*, 3845-3897. [3] Grady, M. M. (2001) Catalogue of meteorites, Cambridge University Press. [4] Keil, K., and Bell, J. F. (1992) *Icarus*, 98, 43-53. [5] Kuebler E. K. et al. (2006) *Geochim. Cosmochim. Ac., 70*, 6201–6222. [6] Fries, M. et al. (2011) *CORALS II* abstract#4087. [7] Scott, E. R. D., Sharma, S. K, and Chio, C. H. (2004) *GEORAMAN 2004*, 61-62. [8] Chen, M. et al. (2007) *Earth Planet. Sci. Lett, 264*, 277–283 [9] Yu, Y. G., and Wentzcovitch, R. M. (2006), *J. Geophys. Res. 111*, B12202. [10] Nagy, S. et al. (2010) *LPSC 41*, Abstrac# 1228 [11] Nagy, S. et al. (2010) AMRC Symp.XXXIII. [12] Chopelas, A. (1991) *Amer. Mineral., 76*, 1101-1109. [13] Lam, P. K., et al. (1990) *Amer. Minerat,75*, 109-119. [14] Kuebler, K. E. et al (2006) *Geochim. Cosmochim. Ac. 70*, 6201–6222. [15] Rauch, M. et al. (1996) *Amer. Mineral. 81*, 1289-1292.